Numerical Investigation of Film Coefficient Engineering Model for Chemically Reacting Boundary Layers

Justin Cooper,[*]

NASA Johnson Space Center, Houston, TX 77058

Giovanni Salazar,[†]

Corvid Technologies, Mooresville, NC 28117

and Alexandre Martin[‡]

University of Kentucky, Lexington, KY 40506

Aerothermal analysis of spacecraft planetary entry is heavily dependent on heritage engineering models. The film coefficient heat transfer model examined in this paper estimates the convective heating to the vehicle for a laminar, chemically reacting boundary layer for an Earth atmosphere. This model requires information about the vehicle and flow field for a given trajectory point and estimates a proportional relationship between enthalpy potential and convective heat flux. In practice it is the aerothermal engineer who must decide which assumptions are appropriate for their application. This work looks at numerous CFD simulations for an arbitrary, axisymmetric flight vehicle to analyze the relative importance of both the mass and energy constraints imposed at the wall boundary, as well as the effect of various diffusion models. Within the subset of tested energy boundary conditions, it is found that the most desirable energy boundary condition is the radiative equilibrium boundary condition, which permits conservative estimates of convective heat flux, but also generates flow field dependent spatial thermal distributions along the surface. Other key findings are presented in an effort to make the film coefficient engineering model readily available to design engineers across industry.

[*]Aerosciences Division / Graduate Research Assistant, Mechanical & Aerospace Engineering, University of Kentucky
[†]Aerospace Engineer
[‡]Professor, Mechanical & Aerospace Engineer, Associate Fellow AIAA

Nomenclature

$\dot{\omega}$ Production rate of chemical species i [kg/m^2/s]

ϵ Surface emissivity of a given material

η Surface normal coordinate [m]

γ^* Ratio of specific heats evaluated at the reference temperature/enthalpy

γ_i Accommodation coefficient of chemical species i

$\gamma_{i,0}$ Reaction probability of chemical species i

$\mathbf{F}$ Diffusive flux vector

ρ Fluid mixture density [kg/m^3]

ρ_w Fluid density at the vehicle wall [kg/m^3]

σ Stefan-Boltzmann constant [W/m^2/K^4]

τ Shear stress tensor

$\mathrm{C_H}$ Stanton number

$\mathrm{C_M}$ Mass transfer coefficient

Le_i Lewis number for chemical species i

Pr Prandtl number with properties evaluated at fluid temperature

Pr^* Prandtl number with properties evaluated at reference temperature/enthalpy

c_p Specific heat of fluid [J/kg/K]

D Mixture mass diffusion coefficient [m^2/s]

D_i Mass diffusion coefficient of chemical species i

e Subscript indicating location at the boundary layer edge

h Total enthalpy [J/kg]

h_0 Stagnation enthalpy [J/kg]

h_e Static enthalpy at the boundary layer edge [J/kg]

h_r Recovery enthalpy [J/kg]

h_{aw} Adiabatic wall enthalpy [J/kg]

i Subscript referring to chemical species i

j_i Mass diffusion flux for chemical species i

k Thermal conductivity [W/m/K]

M_e Mach number evaluated at the boundary layer edge

M_i Molecular weight of chemical species i [kg/mol]

M_∞ Freestream Mach number

P_w Pressure at the wall [Pa]

American Institute of Aeronautics and Astronautics

q_{cond}	Conduction heat flux [W/m^2]
q_{rad}	Radiation flux from the fluid to the wall [W/m^2]
R	Universal gas constant [J/K/mol]
r	Recovery factor, non-dimensionalized adiabatic wall enthalpy/temperature
T_e	Temperature at the boundary layer edge [K]
T_w	Vehicle wall temperature [K]
T_∞	Far-field radiation temperature [K]
T_{ac}	Activation temperature [K]
u_e	Velocity at the boundary layer edge [m/s]
v_w	Surface normal velocity at the vehicle wall [m/s]
w	Subscript indicating location at the vehicle wall
$X_{k,\infty}$	Mole fraction of chemical element k at the freestream condition [mol/mol]
Y_i	Mass fraction of chemical species i [kg/kg]
CFD	Referring to a quantity computed in the computational fluid dynamic simulation
EQ	Referring to chemical equilibrium
MR	Referring to a quantity computed in the material response simulation
NE	Referring to chemical non-equilibrium

I. Introduction

In aerothermodynamics, the principle quantities of interest are the surface heat flux and the time-integrated heat flux (heat load). For hypersonic vehicles entering an atmosphere, coupling the fluid flow field and the thermal response analysis into a single computational simulation best incorporates all of the strongly interacting physics. Numerous examples exist in the literature of coupling approaches.[1–5] However, when designing a vehicle, it is preferred for the two domains to be decoupled. Because the vehicle will undergo many changes during the process of designing and building, engineers need to have models available that can react to those changes. This makes the larger computational effort of a fully coupled approach less ideal.

To accomplish this decoupling, the film coefficient engineering model[6–11] is used. Information from the flow field is transferred as a boundary condition to the material response solver. In this manner, the model estimates the convective heating to the vehicle, but becomes sensitive to assumptions made in the CFD simulation. This paper analyzes the assumptions of the models, as well as their effect on the resulting heat transfer.

The film coefficient nomenclature has a historical precedence in heat exchanger theory,[12] where it was

first used to linearize the temperature relationship in close proximity to the wall. Today, it is associated with transfer coefficient methodology, which extends to all of the boundary layer equations (mass, momentum, and energy). The transfer coefficients for each of the governing equations are a consequence of simplifying the equations to a similar form where only the advective and diffusive fluxes exist. Under these conditions, if the mass flux of the fluid approaches zero at the wall, then a linear proportionality constant may be defined which governs the relationship between the conserved quantity's gradient and the driving potential. The driving potential is most often the difference between the conserved quantity at the boundary layer edge and the wall. See Spalding[13] or Kays and Crawford[14] for these details.

Based on this knowledge of the diffusive flux relationship to the transfer coefficients, their definition and relationship to one another may be usefully illustrated. The diffusive fluxes take the form

$$\mathbf{F} = (j_i, \tau, q_{\mathrm{cond}})^T .$$

$$(1)$$

For this paper and forthcoming research on the topic, the relationship between the fluid conduction and mass diffusion is derived. The mode of energy transfer by molecular collisions within the gas is known as conduction, and in high velocity flows subject to real gas effects, is modeled using Fourier's Law

$$q_{\mathrm{cond}} = -\frac{k}{c_p}\frac{\partial h}{\partial \eta}$$

$$(2)$$

where k is the thermal conductivity of the media, c_p is the specific heat at constant pressure, h is the total enthalpy, and η is the surface normal direction. The mass exchange due to molecular collisions is modeled by Fick's Law

$$j_i = -\rho D_i \frac{\partial Y_i}{\partial \eta}$$

$$(3)$$

where ρ is the mixture density, D_i is the species diffusion coefficient, and Y_i is the mass fraction of species i. Taking the ratio of Eq. 2 to Eq. 3 and using the chain rule gives

$$\frac{q_{\mathrm{cond}}}{j_i} = \frac{k}{\rho D_i c_p}\frac{\partial h}{\partial Y_i}.$$

$$(4)$$

The definition of the species Lewis number is given by

$$\mathrm{Le}_i = \frac{\rho D_i c_p}{k}.$$

$$(5)$$

The Lewis number refers to the ratio of thermal versus mass diffusivity. At this point in the derivation, the assumptions of thin film theory must be employed. Assume that the boundary layer is thin enough that

its properties remain constant, including its height. Integrating across the boundary layer height δ, Eq. 4 becomes

$$\int_{Y_{w,i}}^{Y_{e,i}} \frac{\text{Le}_i}{j_i} dY_i = \int_{h_w}^{h_e} \frac{1}{q_{\text{cond}}} dh. \tag{6}$$

Computing the integral and rearranging then yields

$$\frac{q_{\text{cond}}}{h_e - h_w} = \frac{1}{\text{Le}_i} \frac{j_i}{Y_{e,i} - Y_{w,i}} \tag{7}$$

where all of the properties comprising the Lewis number have been assumed constant but not necessarily at the wall state (discussed later). The subscript w refers to the wall boundary and e refers to the boundary layer edge. Letting the species diffusion coefficients be equal, such that $D_i = D$, permits the dropping of the i notation associated with a single species in both the mass diffusion flux and the mass fraction terms. Normalizing by the mass flux at the boundary layer edge gives

$$\frac{q_{\text{cond}}}{\rho_e u_e (h_e - h_w)} = \frac{1}{\text{Le}} \frac{j}{\rho_e u_e (Y_e - Y_w)} \tag{8}$$

or simply

$$\text{C}_{\text{H}} = \frac{1}{\text{Le}} \text{C}_{\text{M}}. \tag{9}$$

The value on the left hand side of Equation 9 is the Stanton number and the quantity on the right is the mass transfer coefficient divided by the Lewis number. In other words, according to thin film theory the heat and mass transfer coefficients are related to one another through the Lewis number. This exact same procedure may be applied to any of the two diffusive flux components, with the resulting relationship being governed by either the Schdmit, Prandtl, or Lewis number. By letting $\text{Le} = 1$ the heat and mass transfer coefficients are equated. This is the so-called heat and mass transfer analogy, and becomes relevant for cases where mass transfer processes are occurring at the surface.

For a high velocity gas with freestream Mach number $M_\infty >> 1$, two physical phenomena must be accounted for in engineering correlations; the first is viscous dissipation, and the second is the real gas effects caused by the high temperatures. It has been found that the effect of viscous dissipation may be included in low speed engineering correlations by simply inserting the adiabatic wall value (either temperature or enthalpy) instead of the boundary layer edge value. To compute the adiabatic wall value, the recovery factor definition must be introduced.

$$r = \frac{h_{aw} - h_e}{u_e^2 / 2} \tag{10}$$

A numerical approximation based on boundary layer solutions was first calculated by Pohlhausen[16] and later extended by Eckert[18] for the laminar boundary layer. The traditionally used recovery factors for laminar

and turbulent flows are given by Equation 11, which may be found in Dorrance[17] or in the original Eckert paper.[18]

$$r = \begin{cases} \Pr_*^{1/2}, & \text{laminar}, & 0.5 < \Pr < 5.0 \\ \Pr_*^{1/3}, & \text{turbulent}, & \Pr \approx 1 \end{cases} \tag{11}$$

These engineering correlations permit an evaluation of the adiabatic wall value based solely on the fluid properties. Since the specific heat in a hypersonic flow will vary with temperature, the film coefficient engineering model is defined in terms of the recovery enthalpy

$$h_r = h_e + r\frac{u_e^2}{2}. \tag{12}$$

In Equation 12, it seen that the adiabatic wall enthalpy from Equation 10 is replaced by the recovery enthalpy, as the *approximation* of the recovery factor is used in place of the exact value.

The change in energy potential, however, does not include real gas effects caused by high temperatures in the boundary layer. To account for this variation, Eckert[12, 19] promoted the reference method, which was originally set forth by Rubesin and Johnson.[20] This method posits that if the variable fluid properties are evaluated at a *reference* temperature or enthalpy, that the constant property relationships for convective heat transfer may be applied. Examining Equation 11, the $\Pr_*^n$ term refers to the Prandtl number calculated at the reference temperature or enthalpy. Where evaluated, the reference temperature in this work is computed using Eckert's model

$$T^* = 0.4T_e + 0.6T_w + 0.11r\left(\gamma^* - 1\right)M_e^2. \tag{13}$$

In Equation 13, T_e is the temperature at the boundary layer edge, T_w the wall temperature, r the recovery factor, γ^* the ratio of specific heats evaluated at the reference temperature, and M_e is the Mach number at the boundary layer edge. However, Van Driest has shown[21] very little variation in the computed recovery factor for the case of a flat plate in air at hypersonic speeds. For the purposes of this paper it is assumed to have a constant value of $r = 0.85$, which is just under the $\Pr^{1/2}$ value shown in the Van Driest paper.

Applying both the recovery model and reference method to the definition of the Stanton number gives the *hypersonic* film coefficient

$$\rho_e u_e C_{\mathrm{H}} = \frac{q_{\mathrm{cond}}}{(h_r - h_w)} \tag{14}$$

where the driving potential in the denominator is $h_r - h_w \approx h_{aw} - h_w$ and the Prandtl number model used for the recovery enthalpy is evaluated at the reference temperature/enthalpy. Equation 14 is the historical film coefficient engineering model, which through the assumption of a unity Lewis number has separated/neglected mass diffusion effects.

Note that the film coefficient differs from the Stanton number, as it is a *dimensional* transfer coefficient. Historically, the Nusselt number (a dimensionless quantity) has been used to report heat transfer results. Non-dimensional relationships are essential for comparison of theory to experimental results across a wide range of conditions. However, the hypersonic film coefficient is a transfer coefficient in units of $\text{kg/m}^2/\text{s}$. This metric is preferred due to the extension of the model to systems which include mass injection at the surface. These systems undergo considerable simplification by non-dimensionalizing the mass flux terms, see for example Bianchi.[22] They will be described in a future paper.

Section II will elaborate on how the film coefficient model is calculated using CFD, as well as detailing the assumptions tested in the model framework. Section III presents a numerical experiment for a hypothetical vehicle at a representative flight condition. Section IV summarizes the main results of the analysis in the previous section and lists future areas of study for this line of research.

II.   Modern Film Coefficient Engineering Model

One of the biggest advantages of the film coefficient model is being able to predict the heating to the vehicle over a range of wall conditions based on a single CFD solution. A description of how the variables of the model are computed is first described. The construction of a boundary condition and its use in the material response solver is then shown.

Model description

The implementation of the film coefficient engineering model begins by computing the flow field of the vehicle for a given trajectory point. For the instance of this study, we consider a fully viscous, chemically reacting system of conservation equations. The film coefficient may be calculated at a given body point on the vehicle as

$$\rho_e u_e C_{\text{H}}^{\text{EQ}} = \frac{q_w^{\text{CFD}}}{h_r^{\text{CFD}} - h_w^{\text{EQ}} \left(T_w^{\text{CFD}}, P_w^{\text{CFD}}, X_{k,\infty}\right)} \tag{15}$$

or

$$\rho_e u_e C_{\text{H}}^{\text{NE}} = \frac{q_w^{\text{CFD}}}{h_r^{\text{CFD}} - h_w^{\text{NE}} \left(T_w^{\text{CFD}}, P_w^{\text{CFD}}, Y_{i,w}^{\text{CFD}}\right)} \tag{16}$$

where q_w^{CFD} and h_r^{CFD} are the wall heat flux and the recovery enthalpy, both computed from the CFD solution. The wall enthalpy h_w may be evaluated as the equilibrium wall enthalpy (h_w^{EQ}), which is the mixture enthalpy evaluated at the wall state using freestream elemental mole fractions ($X_{k,\infty}$). In practice, this requires the use of an external chemical equilibrium solver, as well as the pressure and temperature at the wall as inputs for calculation. The non-equilibrium wall enthalpy (h_w^{NE}) is the weighted sum of the enthalpies of the gaseous species ($\sum_i Y_i h_i$) at the wall in the CFD solution.

To determine the so-called aeroheating boundary condition at the surface of the material response computation, the film coefficient is multiplied by the enthalpy driving potential, yielding

$$q_{\mathrm{EQ}}^{\mathrm{MR}} = q_w^{\mathrm{CFD}} \left[\frac{h_r^{\mathrm{CFD}} - h_w^{\mathrm{EQ}} \left(T_w^{\mathrm{MR}}, P_w^{\mathrm{CFD}}, X_{k,\infty} \right)}{h_r^{\mathrm{CFD}} - h_w^{\mathrm{EQ}} \left(T_w^{\mathrm{CFD}}, P_w^{\mathrm{CFD}}, X_{k,\infty} \right)} \right] \qquad (17)$$

or

$$q_{\mathrm{NE}}^{\mathrm{MR}} = q_w^{\mathrm{CFD}} \left[\frac{h_r^{\mathrm{CFD}} - h_w^{\mathrm{EQ}} \left(T_w^{\mathrm{MR}}, P_w^{\mathrm{CFD}}, X_{k,\infty} \right)}{h_r^{\mathrm{CFD}} - h_w^{\mathrm{NE}} \left(T_w^{\mathrm{CFD}}, P_w^{\mathrm{CFD}}, Y_{i,w}^{\mathrm{CFD}} \right)} \right]. \qquad (18)$$

Superscripts denoted CFD refer to values extracted from the CFD simulation, whereas the superscript MR refers to values from the material response solver. This results in the notation for a non-equilibrium wall enthalpy based heat flux ($q_{\mathrm{NE}}^{\mathrm{MR}}$) and an equilibrium wall enthalpy based heat flux ($q_{\mathrm{EQ}}^{\mathrm{MR}}$). Note that, this is the wall enthalpy in the denominator of Equations 17 and 18 and that the wall enthalpy in the numerator is always computed in chemical equilibrium using the wall temperature from the material response, the wall pressure from the CFD, and the freestream elemental mole composition.

Next, note that the prior derivation of the Stanton number only contains a conduction term in the heat flux. However, in the modern method of computing a film coefficient, *the CFD heat flux contains all of the engineering approximations about the flow field.* This includes mass diffusion energy, vehicle geometry (effects of curvature), entropy swallowing, flow state, etc. The surface energy balance (SEB) for a non-ablating, non-decomposing vehicle surface is given by

$$q_w^{\mathrm{CFD}} = \left[-k_w \frac{\partial T}{\partial \eta} - \sum_i j_i h_i + q_{\mathrm{rad}} \right]_{\mathrm{fluid}} = \left[q_{\mathrm{cond}} \right]_{\mathrm{solid}} + \left[\epsilon \sigma \left(T_w^4 - T_\infty^4 \right) \right]_{\mathrm{surface}} \qquad (19)$$

where the first term on the left is the conduction energy from the gas, the second term is the energy carried by diffusion, and the third is radiation from the gas. On the RHS of Eq. 19 is the solid conduction energy into the material. The remaining term on the RHS is a surface source term, the re-radiation of energy from the solid surface. For a discussion of generalized boundary conditions between CFD and material response, see Martin.[23]

The SEB includes the diffusive energy term and is coupled to the interior of the CFD solution by the mass gradient, as well as the thermal gradient in the conduction term. Based on this observation, a change in the diffusion model of the entire flow field can alter the surface heating. Altering the homogeneous kinetics can also significantly affect this diffusion term as it is a function of mass composition.[24] Frequently employed models for diffusion are constant Lewis number and the Self-Consistent Effective Binary Diffusion (SCEBD) model.[25] The constant Lewis number model requires that the *local* species mass diffusion coefficients be

equal such that

$$D = D_i = \frac{\mathrm{Le}k}{\rho c_p}. \tag{20}$$

A common assumption in boundary layer theory asserts that Le $= 1$, which was primarily used for the convenience of simplifying the fluxes in the energy equation. More realistic, is perhaps the Lewis number value of 1.4, frequently adopted in the literature (for example see Kemp, et. al.[?]). The SCEBD model computes the species mass diffusion coefficients subject to the constraint that all of the fluxes sum to zero.

The diffusion term is also related to the surface chemistry model chosen. The surface mass balance (SMB) for a non-ablating, non-decomposing vehicle surface is given by

$$[-j_i + \rho_w v_w Y_{i_w}]_{\mathrm{fluid}} = [\dot{\omega}_i]_{\mathrm{surface}} \tag{21}$$

where j_i is the species mass diffusion flux, the second term is the advected mass flux, and the term on the right is a surface source term related to the creation or destruction of species at the surface. For a no-slip surface the advection term is exactly zero and thus the chemical source term must equal the diffusion term. This means that the presence of the wall and the surface material's ability to recombine dissociated particles must now be considered in the surface heat flux calculation.

It is Goulard[26] who extended the work of Fay and Riddell[27] and Lees[28] to include the effects of varying wall catalycity, citing the relationship between the chosen wall mass boundary condition and the mass diffusion. Noting Goulard's work, Park presented a model[29] for computing catalytic processes. In the present work, Park's specified reaction efficiency (SRE) model is used to represent surface catalysis. The model computes the production rate $\dot{\omega}$ for a given species i as

$$\dot{\omega}_i = \rho_i \gamma_i(T_w) \sqrt{\frac{RT_w}{2\pi M_i}} \tag{22}$$

where ρ_i is the species density, T_w is the wall temperature, R is the universal gas constant, and M_i is the molecular weight of the given species. The γ_i function is an accommodation coefficient taking the form

$$\gamma_i = \gamma_{i_0} \exp \frac{T_{ac}}{T_w} \tag{23}$$

where γ_{i_0} is the reaction probability ranging from 0 to 1 and T_{ac} is the activation energy divided by the gas constant. When referring to the *fully catalytic* model, $\gamma_{i_0} = 1$ for a given species, excluding nitric oxide. NO is not a recombination product and therefore the production term in the species mass boundary condition is always exactly zero. This also simplifies the system such that the production rates for atomic species are simply the negative of their molecular counterparts.

American Institute of Aeronautics and Astronautics

The Park model is colloquially referred to as *fully catalytic*, however, this particular model does not equate to chemical equilibrium at the vehicle surface. Chung[?] points out that the first order form of Eq. 22 should only be valid up to a wall temperature of 2000 K and at pressures above 10^{-4} atm. Therefore, at increasingly high wall temperatures, the model will predict mass fractions not consistent with chemical equilibrium. It may be inferred from this observation, that a film coefficient with a *fully catalytic* boundary condition (as defined here) may produce an unphysical film coefficient.

Another significant contribution to surface heating may be radiation from the gas. However, as noted by Brandis and Johnston,[30] convective heating is the dominant mode of heat transfer for Earth entries up to velocities of 9.5 km/s. This means for the design of spacecraft traveling slower than this velocity, the radiation from the gas is neglected such that $q_{\text{rad}} = 0$.

To solve the SEB, an additional assumption requires that the heat conducted into the vehicle be neglected, such that $q_{\text{cond}} = 0$. Physically this requires that the convective heating (fluid conduction+diffusion) be equal to the energy re-radiated from the vehicle. This is also physically the case for a vehicle which is well insulated. A perfect insulator does not allow any conduction through the material. Alternatively, it is possible to simply define an isothermal wall temperature. For this study, a *cold wall* case is considered at 300 K, and a *hot wall* case is considered at 5000 K.

Numerically, when the radiative equilibrium boundary condition is employed, Eqs. 19 and 21 are iteratively solved with the previously mentioned assumptions. This results in a 5x5 system of equations which computes the four species mass fractions and the wall temperature as spatial distributions along the vehicle wall. It includes the effect of the chosen diffusion model through the species diffusion coefficients, the effect of the catalytic model through the accommodation coefficient, and the effect of the radiation equilibrium assumption.

To summarize, the following assumptions are tested in that which follows:

- Diffusion model: Le = 1, Le = 1.4, and SCEBD

- Wall enthalpy: Equilibrium, Non-equilibrium

- Mass boundary condition: Non-catalytic, *Fully catalytic* (Park model)

- Energy boundary condition: Isothermal 300 K, Radiative Equilibrium, and Isothermal 5000 K

Boundary condition implementation

To relate the information from the flow field to the thermal response solver, $\rho_e u_e C_{\text{H}}$ and h_r are computed for a given body point and tabulated. The wall pressure is also extracted from the CFD and tabulated. Each entry in the table is a CFD solution computed along the estimated trajectory of the vehicle. Figure 1

American Institute of Aeronautics and Astronautics

provides a visual depiction of the model. The recovery enthalpy is the anchoring point, shown along the x-axis of the figure. The negative of the film coefficient is the slope of the red line. When the material response is performed, the wall enthalpy is evaluated (the blue circle on the x-axis) at the interpolated pressure from the CFD and the wall temperature from the material response solution. Where the wall enthalpy intersects the film coefficient model is the heat flux prescribed at the solver boundary (blue circle on y-axis). This process is repeated for every time step, interpolating resultant fluxes between time steps.
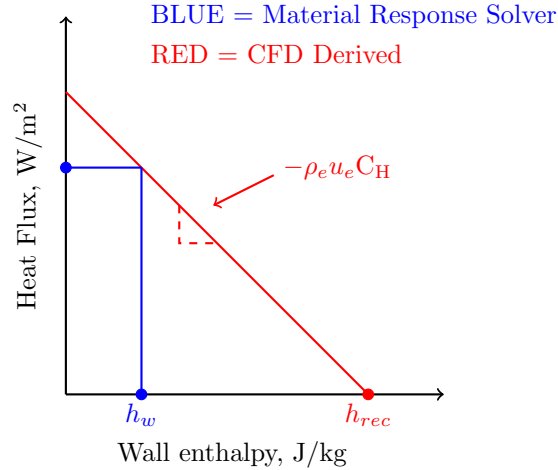
Figure 1: Film coefficient model at a single point in time

With the model now fully described, a numerical case study is presented which assesses the assumptions of the model.

III.   Results and Analysis

Approach

From Equations 17 and 18, it is evident that the computed heat flux (q_w^{CFD}) from the CFD simulation will be a large sensitivity in the downstream material response heat flux ($q_{\text{EQ}}^{\text{MR}}$ and $q_{\text{NE}}^{\text{MR}}$). Regardless of the fidelity of the computational tools being used for the design process, they should be verified and/or validated against higher fidelity methods to develop adequate safety margins for vehicle heating. This is essentially a practice in mitigating the sensititivity associated with the q_w^{CFD} term. Aerothermal margins may be established by comparison of computational tools against experimental data (such as wind tunnel or flight). Alternatively, higher fidelity computational methods may help establish confidence in aerothermal margins dictated for lower fidelity models. The method of determining proper margins is outside the scope of this paper and therefore the sensitivity of q_w^{CFD} is not assessed.

However, a final comment on the q_w^{CFD} term is necessary for the following discussion. The q_w^{CFD} term is

evaluated at a single wall temperature for a given body point in the CFD solution and remains constant. While the *relative value of q_w^{CFD} to reality* is not assessed in this paper, the effect of the chosen wall temperature and the assumed linearity of the model are. The remaining bracketed term in Equations 17 and 18 may then be thought of as a correction factor for the wall temperature assumed by the material response (MR) calculation.

It is useful to analyze each term in a piecewise fashion before examining the cumulative downstream effect on the material response model, since multiple components contribute to the resulting heat flux. This paper examines the *effect of the CFD assumptions on the engineering model* and the subsequent effects on material response analysis. The following effects are discussed:

1. Boundary layer edge properties and recovery factor

2. Chemical equilibrium at the wall

3. Constant film coefficient (functional dependence on h_w)

4. Energy boundary condition (wall temperature)

5. Cumulative effect on material response wall heat flux

Numerical Case Study

To perform the sensitivity study, an arbitrary sphere-shaped flight vehicle of nose radius 2.5 m and point mass of 8000 kg is chosen. A ballistic, non-lifting trajectory at zero angle of attack, with parameters given in Table 1, is modeled using the Kentucky Trajectory Modeling Program (KTMP).[31] The trajectory is chosen so that the peak heating produces significant aerothermal heating without the effects of ionization within the fluid flow.

Parameter	Value	Units
Initial Velocity	6	km/s
Flight path angle	-1	degree
Altitude at interface	125	km

Table 1: Demonstration entry conditions

By using the Sutton-Graves[32] heating indicator for an Earth atmosphere, the altitude and inertial velocity for the peak heating may be estimated. The altitude may be used to compute the freestream mass fractions and temperature using the Standard Atmosphere[33] model. These freestream parameters serve as inputs for the Data Parallel-Line Relaxation[34] (DPLR) CFD simulation. The grid is 2-dimensional, the simulation performed is axisymmetric, and the usual grid convergence practices were followed in resolving flow features.

American Institute of Aeronautics and Astronautics

The body points under consideration for the vehicle are the stagnation point and the 90° shoulder shown in Figure 2. The stagnation point is a unique, high heating location on the body which decelerates the flow, thereby converting inertial energy to thermal energy. The 90° shoulder location is included to illustrate the thermal recovery concept, well described by van Oudheusden,[?] as well as other downstream effects seen by variation of the model parameters. Other simulation parameters in the study are given in Table 2. Non-numerical values given in the table refer to the chosen model, where NASA-9 refers to the equilibrium coefficients being calculated by temperature curve fits from the NASA-9 dataset out of Glenn Research Center,[35] and Gupta-Yos mixing refers to the Gupta-Yos transport coefficient mixture model.[36] The chosen homogeneous model is given by Park[37] 5-species air, which includes the nitric oxide product. Recall that earlier engineering approximations, such as those by Lees and Fay, modeled air as a binary mixture of molecules (N_2, O_2) and their dissociated atoms (N, O). See Park[37] for a description of the homogeneous reaction set. The thermal field is modeled in thermal non-equilibrium with the two temperature model,[38] which permits the expected vibrational excitation that occurs before molecular dissociation.

Parameter	Value	Units
Altitude	32.5	km
Freestream Velocity	4721.19	m/s
Freestream Density	0.0130462	kg/m^3
Freestream Temperature	228.89	K
Initial Mass Fraction [N2]	0.767	kg/kg
Initial Mass Fraction [O2]	0.233	kg/kg
Surface Emissivity	0.88	
Equilibrium Coefficients [K_{eq}]	NASA-9	
Thermal Properties	NASA-9	
Viscosity Model	Gupta-Yos mixing	
Thermal Conductivity	Gupta-Yos mixing	
Flow State	Laminar	

Table 2: CFD parameters for 5 species case

A.   Boundary layer edge properties and recovery factor

Figure 3 shows boundary layer edge temperature, Mach number, static enthalpy, and recovery factor. Two extremes of the chosen modeling assumptions, the SCEBD diffusion model with a fully catalytic wall at 300 K and the Lewis number unity, non-catalytic wall at 5000 K, are chosen to distinguish that the boundary layer edge properties are insensitive to modeling assumptions.

At the stagnation point of the vehicle, the flow field has decelerated outside of the boundary layer to approximately zero. Due to this same deceleration, the static enthalpy is at a maximum at the stagnation
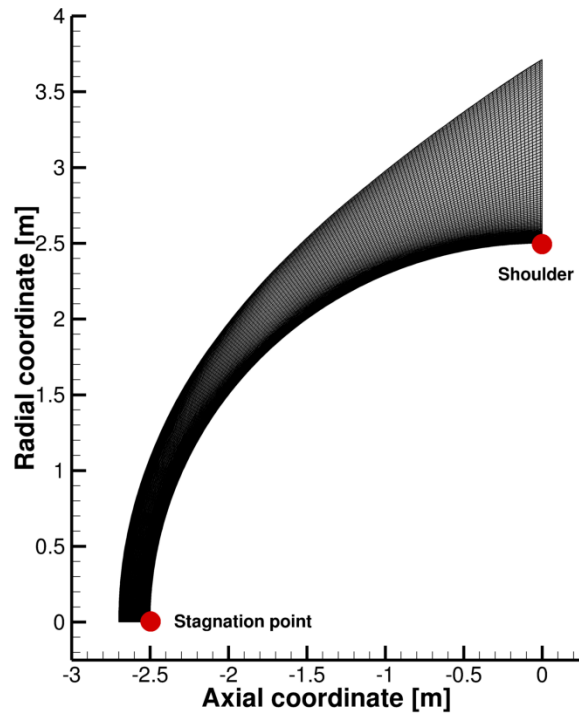
Figure 2: Adapted grid resolution and evaluated body points for test vehicle

point and the Mach number is zero. Along the running length of the vehicle, the increasing Mach number reflects the kinetic contribution to the total enthalpy. The slight increase in enthalpy approaching the shoulder for the 5000 K isothermal wall assumption is due to the vehicle being hot enough to heat the boundary layer in that area (i.e. the conduction term in the SEB is negative). This also appears as a reduction in the edge Mach number.

The change in recovery factor, a function of both wall and edge properties, is less than 0.005 across the body of the vehicle. The insensitivity of the recovery factor is not due to the calculation of the reference temperature, but rather due to the Prandtl number approximation. This is because the properties comprising the Prandtl number behave in similar ways with increasing temperature and tend to compensate for one another. The fall off seen close to the stagnation point is a numerical artifact. The theoretical value of the recovery factor should be exactly equal to unity at the stagnation point, as all of the thermal energy is recovered due to deceleration in the flow. Therefore, in the vicinity of the stagnation point there is a discrepancy between the Prandtl number approximation and the theoretical value, which is not considered further.

The non-dimensional recovery enthalpy is given by

$$h_r^* = \frac{h_r}{h_0} \tag{24}$$

American Institute of Aeronautics and Astronautics
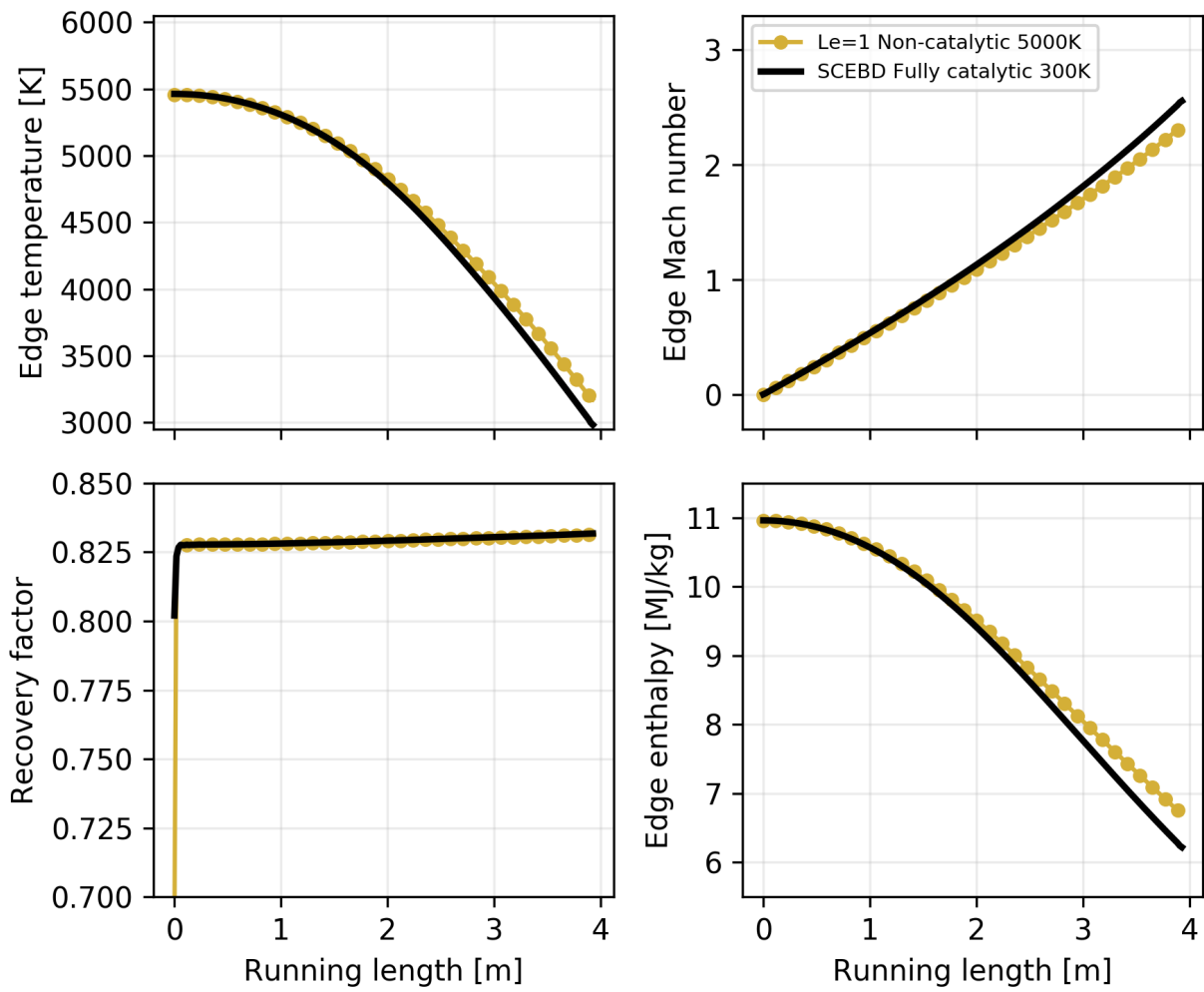
Figure 3: Boundary layer edge properties
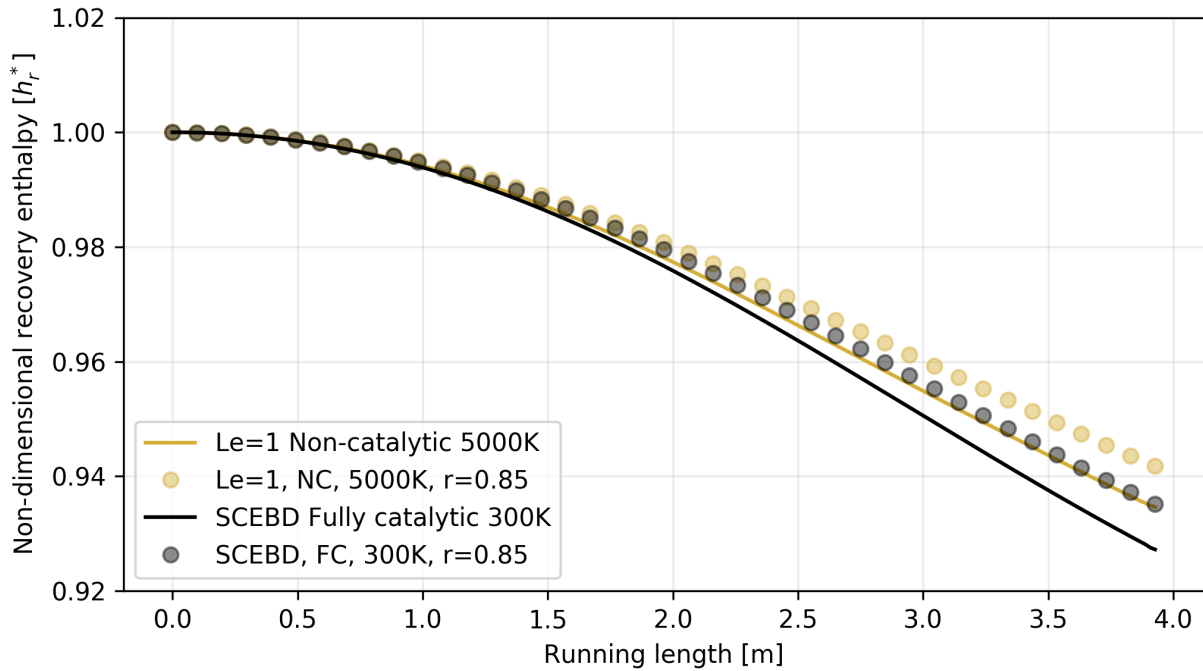
Figure 4: Recovery enthalpy distribution along the boundary layer edge

where h_0 is the stagnation enthalpy, as a function of the running length of the vehicle wall. The two limiting cases are plotted in Figure 4, with and without a constant recovery factor of $r = 0.85$. In the region close to the stagnation point, there is no discernable difference in recovery enthalpy. As the conditions change along the running length of the vehicle, the two limiting extremes diverge by at most 2% at the shoulder. This small variation in recovery enthalpy justifies the assumption of a constant recovery factor.

Examining Figure 5 gives the mass composition as it has reached the boundary layer edge. Again, the two extremes of modeling assumptions are chosen to demonstrate the relative insensitivity to the diffusion model and wall assumptions. However, it is also important to note that the edge properties will vary with respect to the running length of the vehicle. It is seen that the molecular oxygen is nearly fully dissociated at the stagnation point, and the degree to which it is dissociated decreases as the temperature decreases in the running length direction. The discrepancy in the extent of dissociation of molecular oxygen between the two models is the reason for the disagreement in the edge *static* enthalpy (seen in Figure 3) at the shoulder compared to the stagnation point. The amount of NO lost at the shoulder, in concert with decreasing levels of O and N results in a higher percentage of molecular oxygen and nitrogen in that location.

While the recovery enthalpy does not change significantly across the boundary layer edge (approximately 6%), the edge temperature (top plot, Figure 3) and the edge mass fractions (Figure 5) change significantly. These quantities will determine the overall thermal and mass gradients which control the conduction and

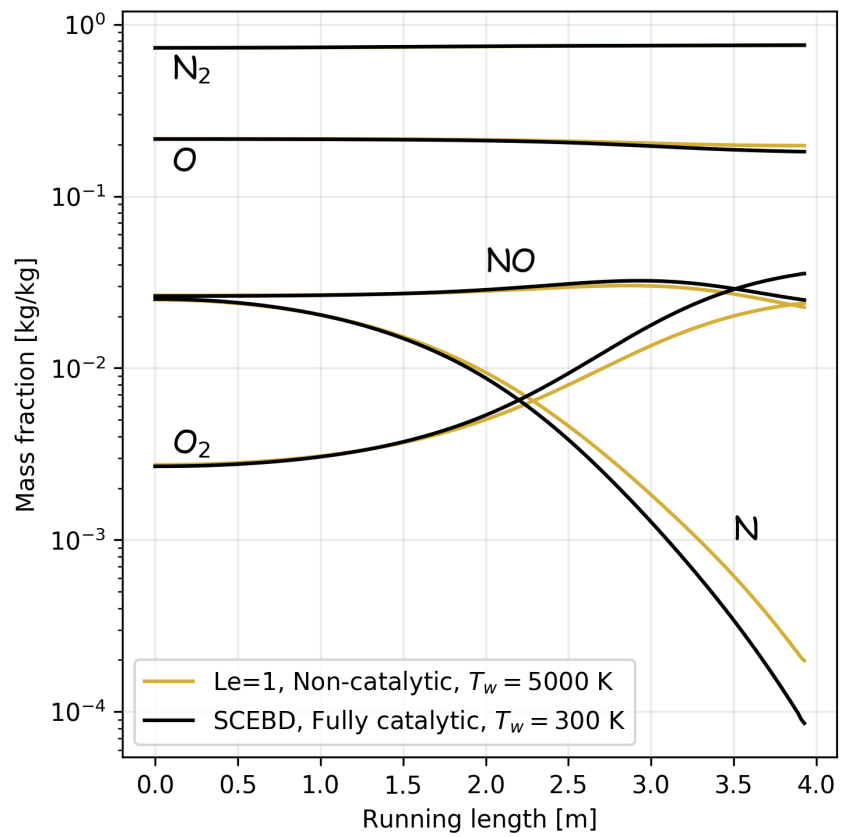American Institute of Aeronautics and Astronautics

Figure 5: Boundary layer edge mass fractions

mass diffusion terms in the SEB.

It is concluded from the above analysis that (for this flight condition, for a given body point) the engineering model is not sensitive to the boundary layer edge properties, except in the case of the hot wall at the shoulder, and that an assumed constant recovery factor value will not skew the results.

B. Chemical equilibrium wall enthalpy assumption

In hypersonic viscous flow, high velocity fluid undergoes rapid viscous dissipation in the boundary layer, which generates a large amount of heat. In this highly energized state, it is appropriate to use enthalpy as an energy metric of the flow due to variable thermodynamic properties (namely specific heat). The heat transfer now becomes functionally dependent upon the mass composition.
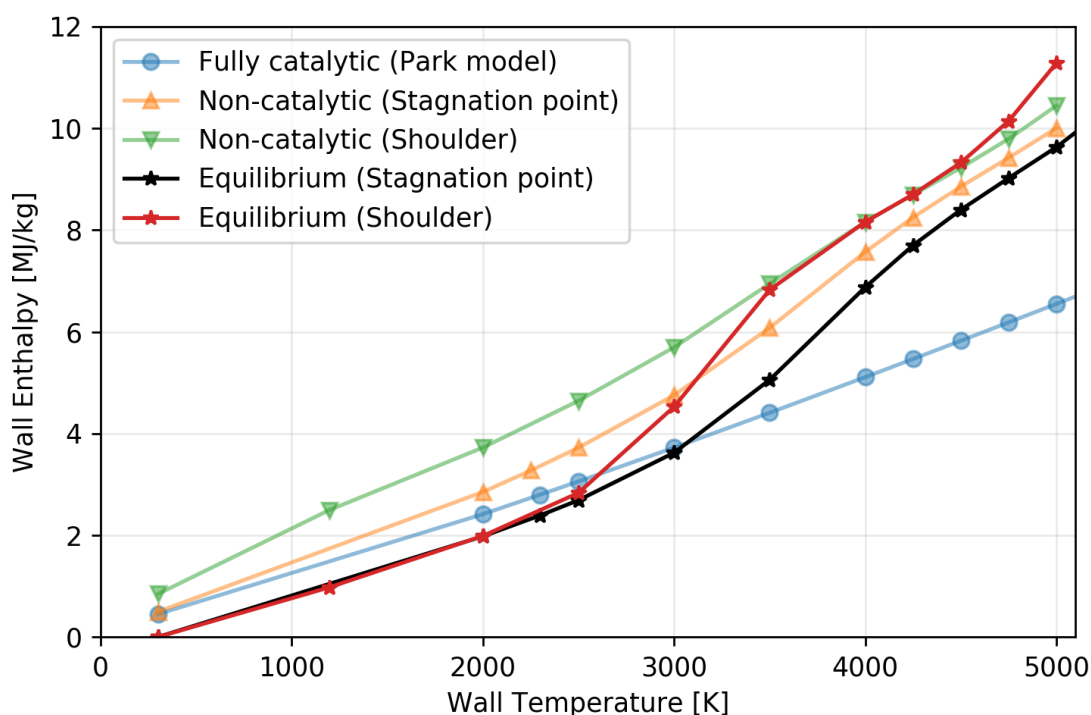
Figure 6: Mass boundary condition effect on wall enthalpy for Earth atmosphere

Figure 6 shows the wall enthalpy as a function of wall temperature for an equilibrium 5-species air mixture at $P = 2.77798 \times 10^5$ Pa (black, stagnation point) and at $P = 1.0476 \times 10^4$ Pa (red, shoulder). Also included are a non-catalytic CFD based wall enthalpy for both the stagnation point (orange) and the shoulder (green), and a CFD based wall enthalpy computation based on the wall species when a *fully catalytic* Park model is implemented (blue, stagnation point).

The wall enthalpy for each of the three models is monotonically increasing with respect to wall temperature. At low wall temperatures (for example 300 K), the non-catalytic and *fully catalytic* mass boundary

American Institute of Aeronautics and Astronautics

conditions permit an appreciable amount of nitric oxide to reach the wall, thereby slightly increasing the wall enthalpy. Additionally, because of the first order nature of the *fully catalytic* model, it takes on a linear form, lacking the curvature of the other two models. This means forcing molecular recombination in a physically inconsistent manner, which results in much lower wall enthalpies at high wall temperatures. The equilibrium wall enthalpies both display a curvature at moderate wall temperatures, reflecting the point where atomic species increase in the mixture. However, since the chemical time scale is finite for a non-catalytic wall (which relies on kinetic mechanisms in the homogeneous phase), there is only one wall temperature range where the shoulder body point reaches equilibrium using the non-equilibrium rates. The stagnation point never fully reaches the chemical equilibrium state.

Figure 7 shows the quantitative species comparison between the kinetic and equilibrium compositions. Figure 7(a) is for the stagnation point of the vehicle and Figure 7(b) is for the shoulder. The percentages are calculated by

$$\frac{\left(X_{i,w}^{\mathrm{CFD}} - X_i^{\mathrm{EQ}}\right)}{X_i^{\mathrm{EQ}}} \times 100.0 \tag{25}$$

where X_i^{EQ} is the equilibrium species mole fraction based on freestream elemental mole composition and i is a given chemical species. The wall boundary condition is chosen to be the hot wall at 5000 K to allow a maximum amount of energy through the boundary layer, in an effort to artificially drive the homogeneous rates as close to equilibrium as possible.

Under these conditions, the stagnation point species' relative error with respect to the equilibrium mole fraction is within 3% for each species. This corroborates the small difference at 5000K in Figure 6, between the orange and black lines. Looking to Figure 7(b), a larger variation from equilibrium composition at the shoulder reinforces the observed behavior of the non-catalytic wall enthalpy seen in Figure 6 (green line) versus the equilibrium enthalpy (red line). The large excess of atomic nitrogen, N, and the smaller percentages of molecular oxygen and nitric oxide result in a higher mixture enthalpy. The point to be made here, is that even at extremely high wall temperatures and moderate pressures, the homogeneous rates do not reach full chemical equilibrium.

C. Constant film coefficient

This section investigates the assumption that

$$\frac{\partial}{\partial h_w}\left(\rho_e u_e \mathrm{C_H}\right) = const. \tag{26}$$

for a given trajectory point. Since the film coefficient is the negative slope of the heat flux, this implies no curvature is present in the relationship between the wall heat flux and the wall enthalpy. Figure 8 plots

American Institute of Aeronautics and Astronautics
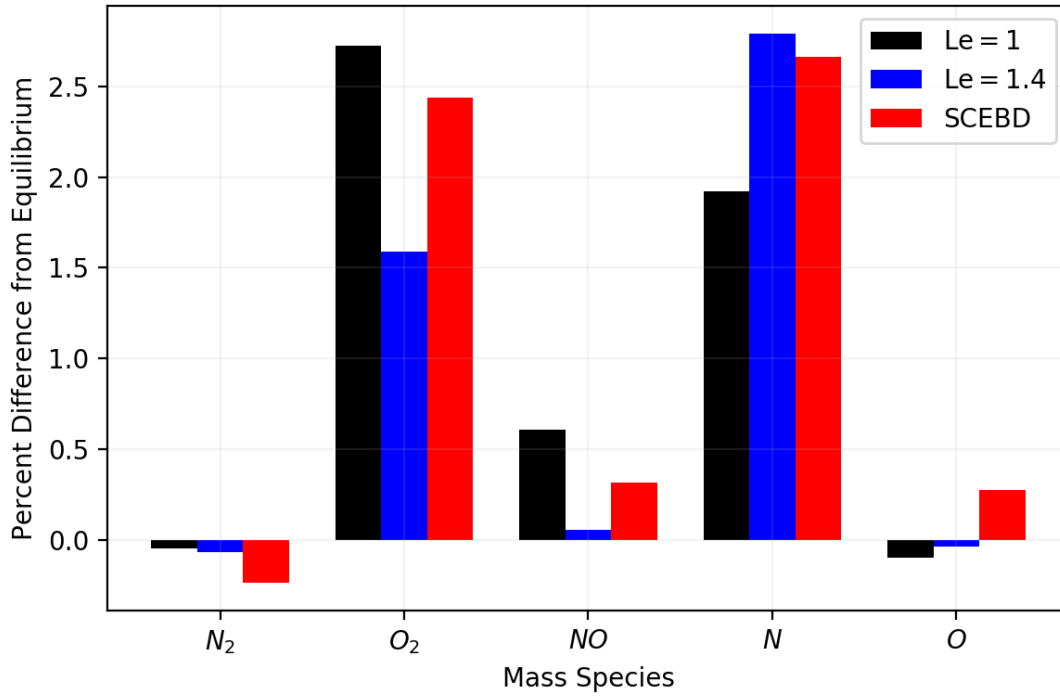
(a) Stagnaton point: $T_w = 5000$ K, $P_w = 2.77798 \times 10^5$ Pa, isothermal wall
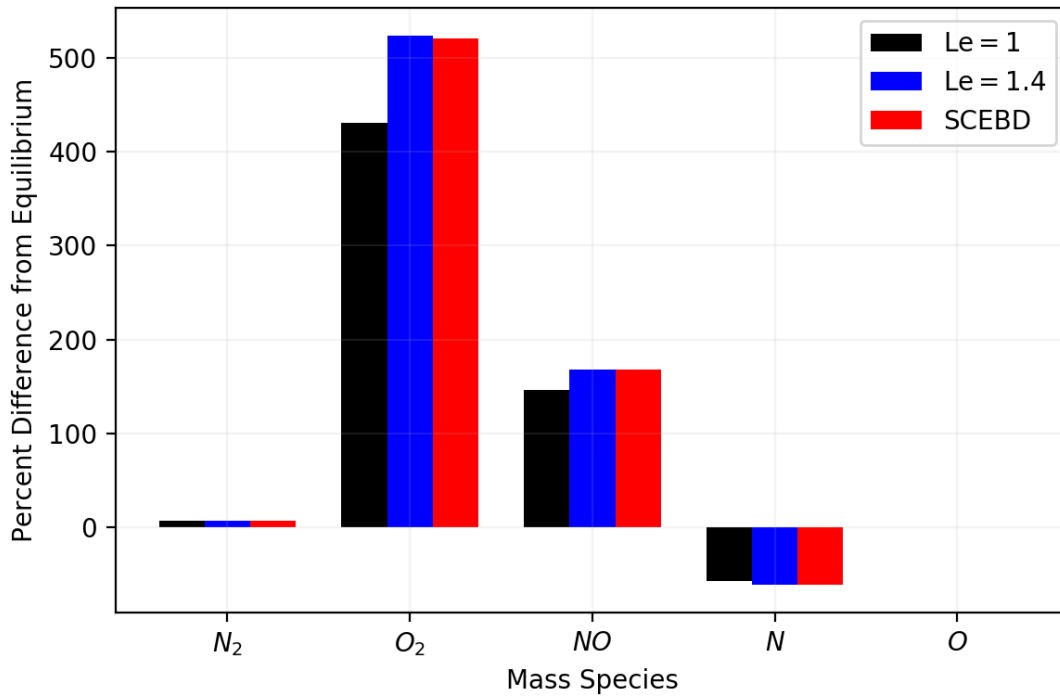
(b) Shoulder: $T_w = 5000$ K, $P_w = 1.0476 \times 10^4$ Pa, isothermal wall

Figure 7: Molar fraction difference of CFD composition vs. equilibrium

the film coefficients for the various diffusion models and mass boundary conditions as a function of the wall enthalpy. Each marker indicates a CFD solution.

Figure 8(a) shows the film coefficients using a non-equilibrium wall enthalpy ($\rho_e u_e C_H^{NE}$, Equation 16). This grouping is intentionally designed to illustrate the effect of adding the diffusive contribution to the surface energy balance (SEB). The solid lines represent a non-catalytic wall, which requires that the source term in the surface mass balance equals zero. This, in turn, nullifies the diffusive term in the SEB, guaranteeing that the total heat flux at the surface is simply the conduction flux. The relative values of the film coefficients between diffusion models may be attributed to their sensitivity to q_w^{CFD}. However, more important, is that when only conduction is considered (solid lines), the increase in non-equilibrium wall enthalpy (see Figure 6) and subsequent decrease in enthalpy potential balances the decrease in the wall heat flux as the wall temperature increases.

In contrast, the dotted lines of Figure 8(a) include the effect of the *fully catalytic* Park model. By this inclusion, diffusion now contributes to the total heat flux at the wall through both the Fick's Law mass diffusion term and the catalytic source term ($\dot{\omega}$). In this instance, the various diffusion models begin to behave differently. For any given wall temperature, the *fully catalytic* model will have an enthalpy potential $(h_r - h_w)$ equal to or less than the non-catalytic model (Figure 6, blue line vs. orange line). At the same time, the q_w^{CFD} term will be affected by the inclusion of the surface mass balance terms. As the wall temperature increases, a decrease in conduction takes place (to the point of heating the boundary layer) coinciding with an increased diffusion contribution. The reason for seemingly disparate behaviors in the three diffusion models is due to *the rate at which the diffusion contribution increases* with respect to wall temperature. For Le = 1 the increase in the diffusion term cannot keep pace with the reduction of heat flux, and therefore the film coefficient decreases. For the SCEBD model, the diffusion outpaces the reduction in conduction, resulting in higher and higher film coefficients. This occurs because the *fully catalytic* Park model has no constraint, where the limiting case should be chemical equilibrium at the wall.

Figure 8(b) shows the film coefficients computed for a film coefficient calculated with an equilibrium wall enthalpy ($\rho_e u_e C_H^{EQ}$, Equation 15). Again, examining the non-catalytic case (solid lines) first, as the case of pure conduction, the lower wall enthalpy compared to a non-equilibrium wall enthalpy allows the reduction in the conduction term to decrease the film coefficients as wall temperature increases. The *fully catalytic* model (dotted lines) demonstrates a large increase in the overall q_w^{CFD} term. In the previous example, the decreasing enthalpy potential (due to the large increase in atoms) helped balance the increasing diffusion contribution. However, in this case, the equilibrium enthalpy potential is much lower, resulting in a large increase in the film coefficients.

In summary, at the stagnation point of the vehicle it may be seen that for a non-catalytic wall, the
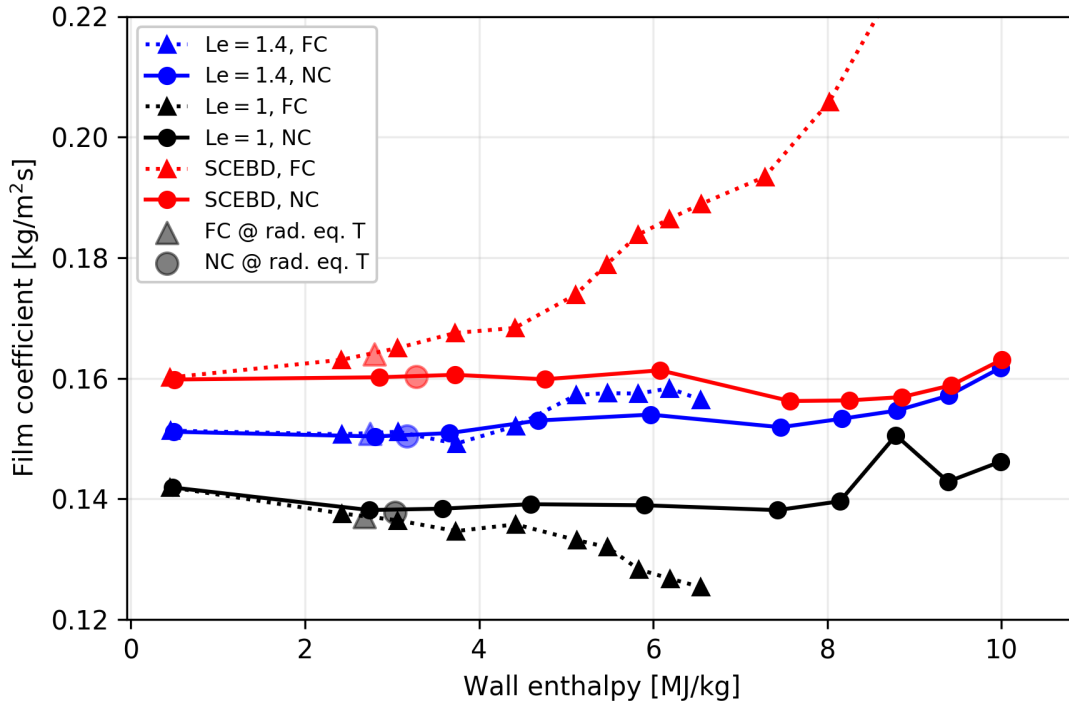
(a) Non-equilibrium wall enthalpy based film coefficients
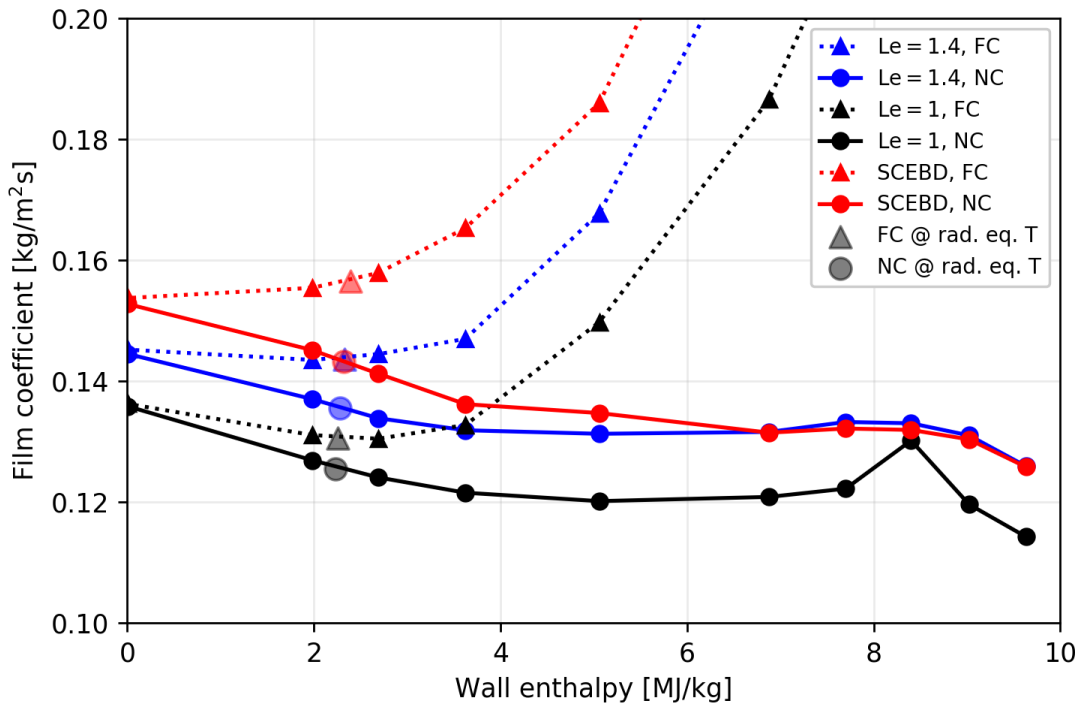
(b) Equilibrium wall enthalpy based film coefficients

Figure 8: Stagnation point film coefficient sensitivity

assumption of a constant film coefficient is a fair approximation of the calculated results. With an equilibrium wall enthalpy, the film coefficient decreases slightly as the wall temperature increases. However, with the implementation of a catalytic model with no energy limit, at high wall temperatures the linearity of the model no longer applies and the film coefficient computation begins to change more rapidly with respect to wall enthalpy.

Figure 9 shows the film coefficients at the $90°$ shoulder as a function of wall enthalpy. Figure 9(a) is the film coefficient computed with a non-equilibrium wall enthalpy ($\rho_e u_e C_H^{NE}$, Equation 16). Notably, all of the film coefficients are an order of magnitude lower than the stagnation point. The thermal energy available in the boundary layer edge has dropped from the stagnation point to the shoulder. This considerably reduces the temperature distribution through the boundary layer and subsequently the thermal gradient at the wall controlling the conduction term. Therefore, for the pure conduction (solid lines), a constant decrease is observed in the film coefficient due to the increase in wall temperature. Eventually, the adiabatic wall temperature is passed and the conduction term becomes negative.

As well, the *fully catalytic* model now does not display the divergent behavior between diffusion models as in the case of the stagnation point. In fact, each of the diffusion models seems to be trending down. Just as the conduction term is smaller due to the edge temperature, so too is the mass diffusion term due to the concentration gradients which exist through the boundary layer height. As evidenced from Figure 3, an increase in molecular oxygen by an order of magnitude from the stagnation point to the shoulder helps keep the diffusion term small. Consequently, the divergence between predicted film coefficients for the *fully catalytic* case is less severe and trending lower with respect to wall enthalpy.

Figure 9(b) shows the film coefficients at the shoulder computed with an equilibrium wall enthalpy ($\rho_e u_e C_H^{EQ}$, Equation 15). The non-catalytic film coefficient (solid line) again reflects the balance between enthalpy potential and computed CFD wall heat flux. After dropping from the cold wall film coefficient (furthest left), the film coefficient becomes approximately constant over a given wall enthalpy range. As the wall state approaches higher energies, the thermal gradient becomes smaller and smaller. Between a wall enthalpy value of 0.8 and 1.0×10^7 J/kg, the vehicle *begins to heat the boundary layer* at the shoulder. However, in the case of the *fully catalytic* model (dotted lines), now the diffusion term in q_w^{CFD} increases faster than the decrease in the conduction term. This results in behavior similar to Figure 8(b). The point where the signs flip for both non-catalytic and *fully catalytic* models indicates that the wall enthalpy has surpassed the recovery enthalpy. For the non-catalytic case this means returning the sign of the film coefficient to positive, while for the *fully catalytic* the film coefficient now becomes negative.

Summarizing the shoulder location, it may be seen that a non-catalytic wall (solid lines) will produce a film coefficient which decreases slightly with respect to wall enthalpy. Approaching the recovery state, it
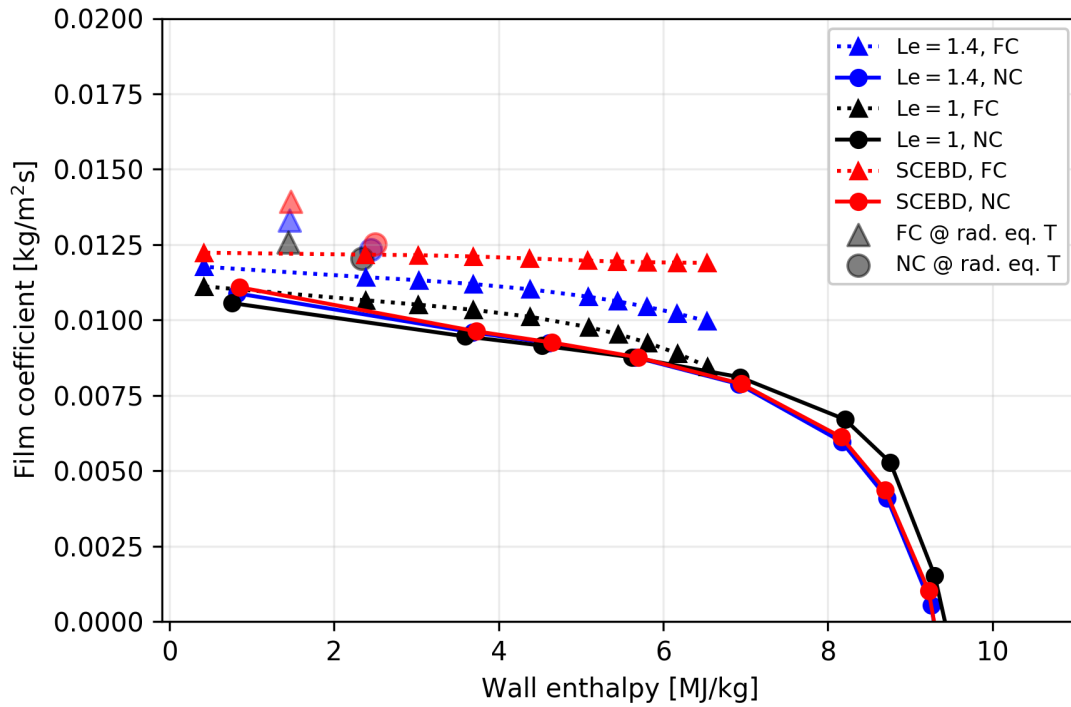
(a) Non-equilibrium wall enthalpy based film coefficients
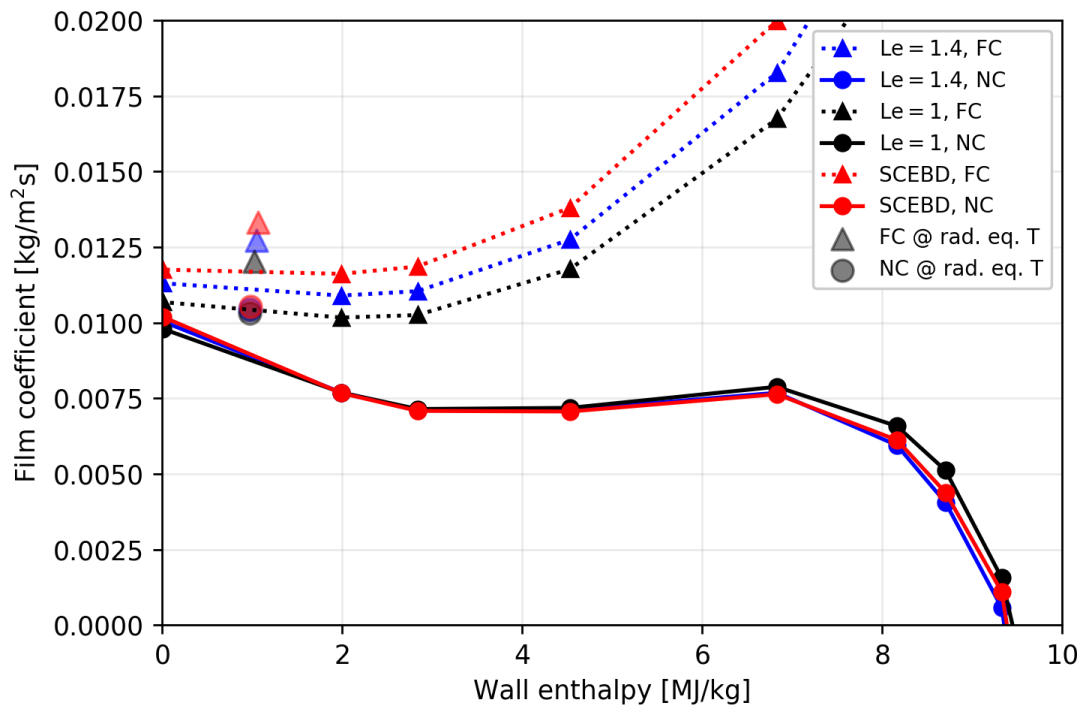
(b) Equilibrium wall enthalpy based film coefficients

Figure 9: Shoulder film coefficient sensitivity

will begin to decrease rapidly, not due to the enthalpy state values' proximity to one another, but due to the conduction term dropping as the wall temperature increases. In the case of the *fully catalytic* model, milder conditions suggest that the divergent behavior seen at the stagnation point is a product of the strong temperature and mass gradients within the stagnation boundary layer. However, the *fully catalytic* model repeats an unphysical behavior seen at the stagnation point when coupled with an equilibrium wall enthalpy.

Finally, it is interesting to note the behavior of the radiative equilibrium wall boundary condition at the shoulder location. Figures 9(a) and 9(b) both have semi-transparent CFD markers for each case. These may be seen between 1-3 MJ/kg in Figure 9(a) and between 0-2 MJ/kg in Figure 9(b). This is a notable feature of the radiative equilibrium boundary condition which creates a thermal distribution as a function of streamwise direction. This leads to a similar thermal distribution as encountered at the boundary layer edge, where the maximum temperature exists at the stagnation point and decreases in the streamwise direction. The transport of upstream energy to downstream body points directly leads to a higher q_w^{CFD}. This is why these CFD markers appear to break the trend of their respective isothermal cases, producing slightly larger film coefficients. This raises the question of which wall energy boundary condition to choose for a given CFD solution, which is investigated next.

D.   Model effect on material response wall heat flux

In Figures 8 and 9 of Section C, each marker represents a given CFD solution for a set of assumptions. A single marker must be chosen to represent the heat transfer for that flight condition. In the previous sections, the entire range of wall temperatures were computed to demonstrate the dependence of the mass boundary condition on the wall energy state. In this section, three energy boundary conditions are employed; a *cold wall* case of an isothermal wall at 300 K, a radiative equilibrium case, and a *hot wall* case of an isothermal wall at 5000 K.

During calculation in the material response code, the only unknown is the wall temperature upon which the h_w^{EQ} depends. In physical terms, if the wall temperature in the material response lags behind the CFD wall temperature (perhaps on the way up the heat pulse), then the result of the model will be to add more heat through the surface. If the vehicle wall is hotter than the evaluated wall temperature in the CFD (perhaps during the convective cooling phase), then the heat transfer will be reduced.

To examine the cumulative impact of the engineering model, the quantities

$$q_{\text{EQ}}^{\Delta} = \frac{q_{\text{EQ}}^{\text{MR}} - q_w^{\text{CFD}}(T_w)}{q_w^{\text{CFD}}(T_w)} \times 100.0 \tag{27}$$

and

$$q_{\text{NE}}^{\Delta} = \frac{q_{\text{NE}}^{\text{MR}} - q_w^{\text{CFD}}(T_w)}{q_w^{\text{CFD}}(T_w)} \times 100.0 \tag{28}$$

may be computed, where $q_{\text{EQ}}^{\text{MR}}$ is the material response heat flux produced by the film coefficient model with an equilibrium wall enthalpy, $q_{\text{NE}}^{\text{MR}}$ is the material response heat flux produced by the film coefficient model with a non-equilibrium wall enthalpy, and $q_w^{\text{CFD}}(T_w)$ is the CFD heat flux, using the same set of assumptions as the film coefficient CFD at the isothermal wall temperature. In other words, this metric computes how close the prediction of the film coefficient model will be to the CFD heat flux, if the CFD were run at the material response wall temperature. Recall, that this does not guarantee the q_w^{CFD} term be close to reality.

In the following figures, the blue lines refer to film coefficient heat flux predictions based on a CFD solution with an isothermal wall at 300 K (or *cold wall*). The orange lines refer to film coefficient heat flux predictions based on a CFD solution with a radiative equilibrium wall, which for these flight conditions corresponds to a spatial distribution in the temperature range [1000-3000] K. The red lines refer to film coefficient heat flux predictions based on a CFD solution with an isothermal wall at 5000 K (or *hot wall*), which approximates an adiabatic wall temperature condition (but permits catalysis). The solid lines in the figure refer to a non-equilibrium (NE) wall enthalpy being used in the denominator of the film coefficient, while the dashed lines refer to an equilibrium wall enthalpy (EQ) based on the state variables at the wall and the freestream elemental mole fractions.

Figure 10(a) is for the non-catalytic wall boundary condition, using the Le = 1 diffusion model. This is consistent with the boundary layer assumption mentioned previously, where heating due to mass diffusion is not present. With conduction as the primary means of heat transfer, Figure 10(a) demonstrates that the film coefficient model will conservatively bound the CFD prediction for all three energy assumptions if the film coefficient is constructed with a non-equilibrium wall enthalpy. On the other hand, the film coefficients constructed with an equilibrium wall enthalpy ($\rho_e u_e C_{\text{H}}^{\text{EQ}}$) predict lower heat fluxes than the non-equilibrium ($\rho_e u_e C_{\text{H}}^{\text{NE}}$) counterparts. This results in areas where the model will underpredict the CFD solution for a given wall temperature.

Figure 10(a) also demonstrates qualitative similarity between the $q_{\text{EQ}}^{\text{MR}}$ and $q_{\text{NE}}^{\text{MR}}$ predictions. Both exhibit an increase from cold wall temperatures up to around 3500 K before reversing curvature. The dip is due to the exponentially decreasing fluid conduction term at high wall temperatures. Further, it is observed that the equilibrium wall enthalpy curves are all lower than their non-equilibrium wall enthalpy counterparts. This result is expected and described in Section B.

Figure 10(b) is for the *fully catalytic* boundary condition at the stagnation point, again using the Le = 1 diffusion model. Most immediately noticeable is the poor performance of the hot wall, equilibrium wall enthalpy film coefficient. This is directly attributable to Chung's observation that a first order catalytic model should not be employed at wall temperatures much higher than 2000K. This results in unphysical mass compositions which deviate strongly from chemical equilibrium.

American Institute of Aeronautics and Astronautics
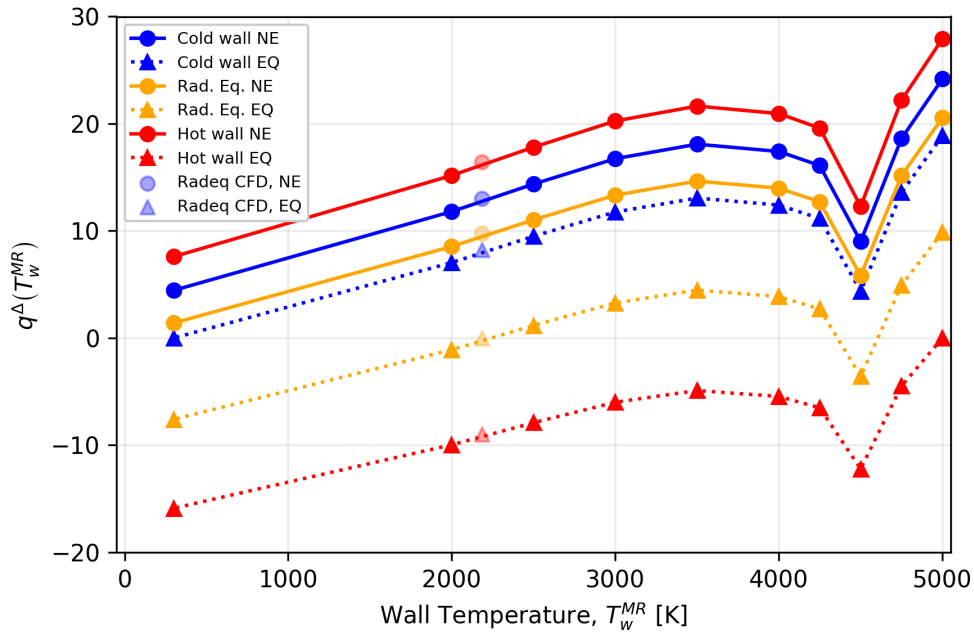
(a) Non-catalytic wall
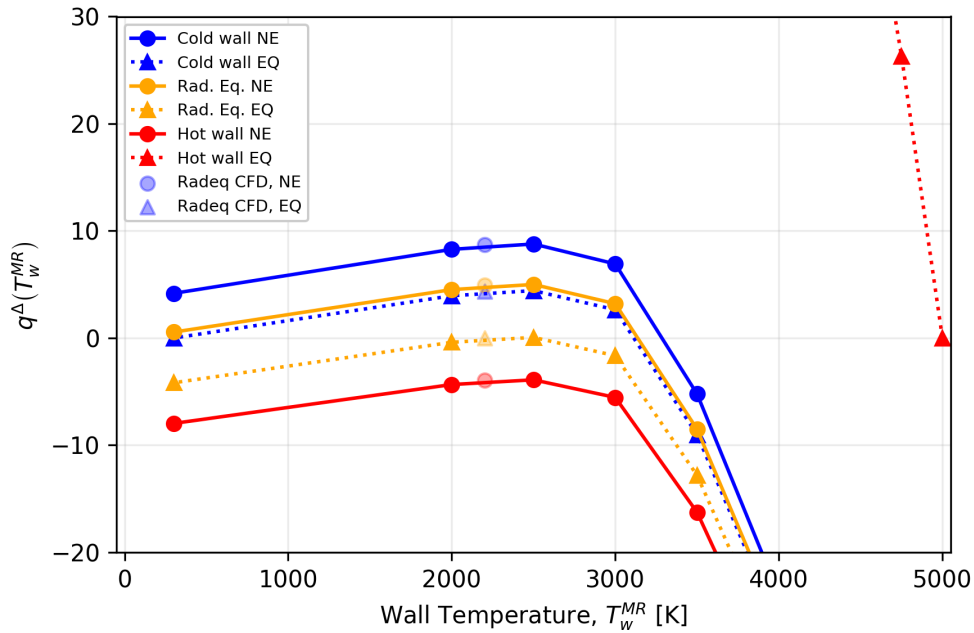
(b) *Fully catalytic* wall (Park model)
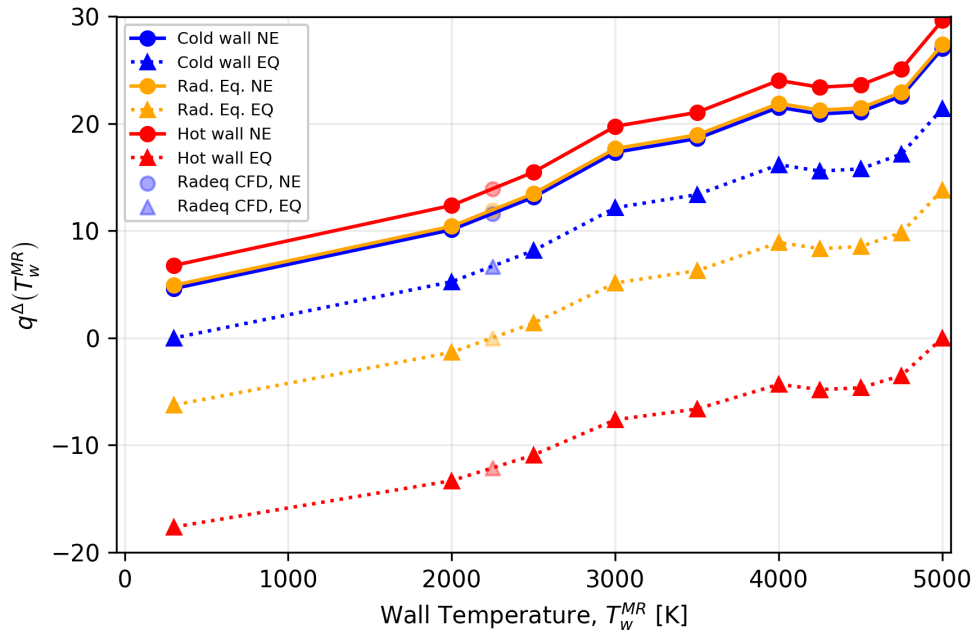
Figure 10: Stagnation point, Le = 1

American Institute of Aeronautics and Astronautics

However, it may be noticed that, at the 5000 K wall temperature, the percent difference is zero. This occurs because the equilibrium wall enthalpy in the denominator of the film coefficient is the same as the wall enthalpy in the numerator. This condition also exists for the cold wall film coefficient (blue) at 300 K and the radiative equilibrium film coefficient between 2000 and 2500 K, and is true for every set of assumptions given only an equilibrium wall enthalpy be used in the film coefficient model.

A qualitative inspection of Figure 10(b) reveals that each of the remaining sets of assumptions gradually increase their prediction of heat flux with respect to wall temperature, reaching a maximum approximately between 2200 and 2500 K. The curvature shifts and the difference of the model against the CFD begins to decrease until at 4000 K it is below 20% of the CFD prediction. This is due to the enthalpy correction term *over-correcting* the CFD predicted heat flux (q_w^{CFD}). However, the film coefficient predictions for each of the sets of assumptions remains within ±10% when below this wall temperature.

Looking to Figure 11, the stagnation point CFD heat flux difference is plotted, now with the SCEBD model. For the case of the non-catalytic wall (Figure 11(a)), unlike the constant Lewis number diffusion model, there is no sharp curvature in between 4000 and 5000 K wall temperatures. Between the two diffusion models, the SCEBD model produces the higher of the two wall heat fluxes, indicating a steeper thermal gradient. This higher gradient at the wall means a less severe decrease in the conduction term, and thus no *dip* in the film coefficient prediction. The *fully catalytic* wall (Figure 11(b)) shares similar attributes to the constant Lewis number, but in the lower to moderate wall temperatures, where the Le = 1 model increases heat flux to a point, the SCEBD diffusion model is monotonically decreasing.

Next, consider the surface heat flux predicted by the film coefficient model at the shoulder location. See Figures 12(a) and 12(b) for the Le = 1 diffusion model. In this case, the hot wall produces applied heat fluxes outside an acceptable range. The cold wall and radiative equilibrium film coefficients produce behaviors similar to the stagnation point location, noting only that now the y-axis range has increased considerably. In Figure 12(a), both wall energy models increase, regardless of enthalpy assumption to a certain point. At the lower pressure shoulder location, the dip previously seen at the stagnation point occurs at a lower temperature. Beyond this critical temperature, the heat flux values from the lower wall temperature CFD solutions become exponentially larger than the material response wall temperatures, resulting in a large amount of conservatism at this body location. Again, the equilibrium wall enthalpy film coefficients produce applied heat fluxes which are lower than their non-equilibrium counterparts for previously mentioned reasons. This body location also demonstrates the radiative equilibrium cumulative effect. The semi-transparent markers are located below their isothermal counterparts. Since the heat flux associated with a radiative equilibrium is *higher* than an isothermal wall case, the difference between the material response wall temperature will be smaller. This results in a smaller prediction of the applied surface heat flux.
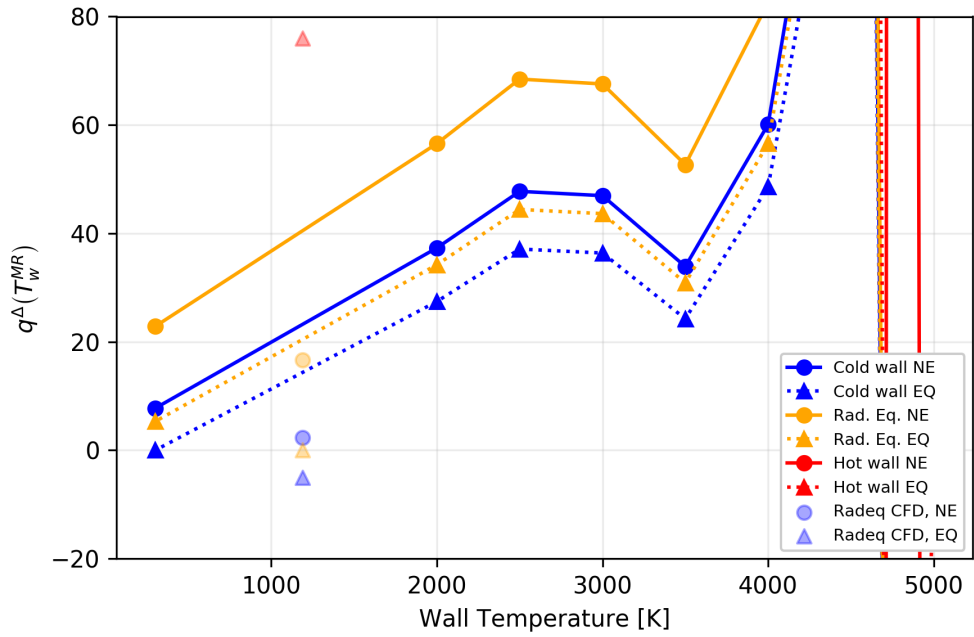
American Institute of Aeronautics and Astronautics
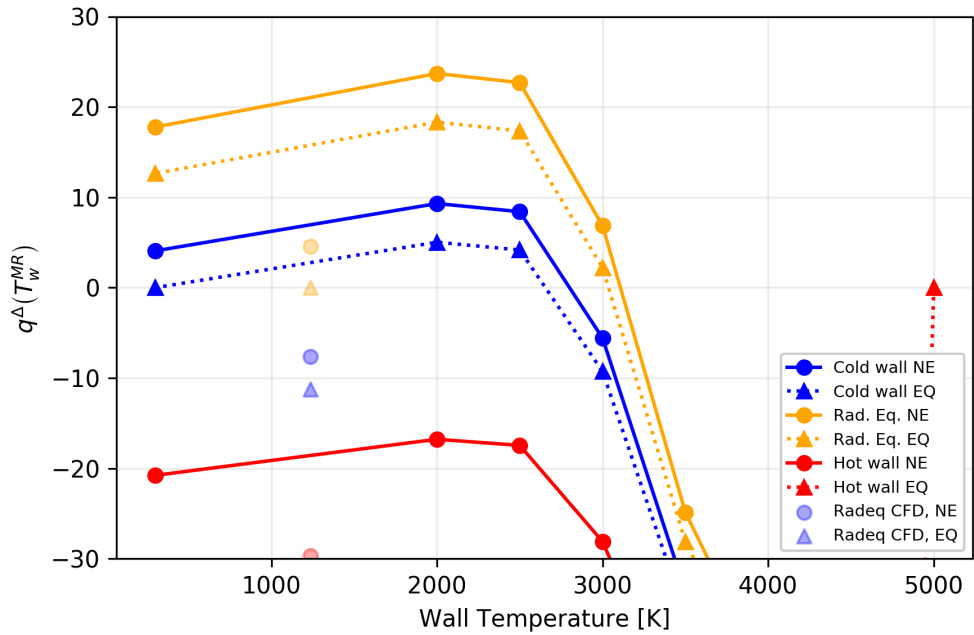
(a) Non-catalytic wall
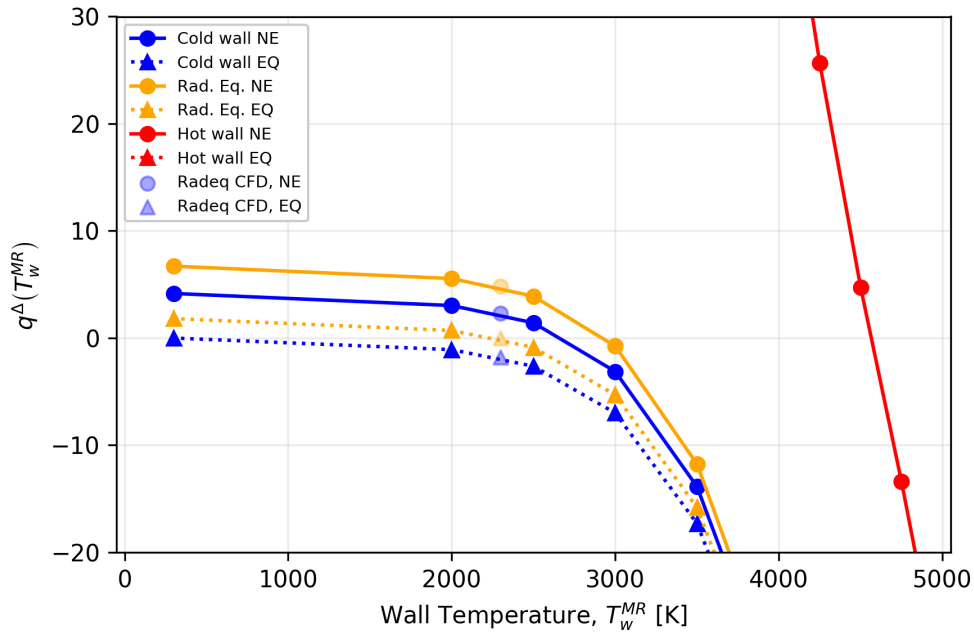
(b) *Fully catalytic* wall (Park model)

Figure 11: Stagnation point, SCEBD model

(a) Non-catalytic wall

(b) *Fully catalytic* wall (Park model)

Figure 12: Shoulder, Le = 1

When the wall is *fully catalytic*, as in Figure 12(b), the behavior is qualitatively similar to the stagnation point. Again, the cold wall and radiative energy conditions increase with respect to wall temperature up to around 2500 K before getting less and less conservative. Again, the radiative equilibrium cases are shown to be lower than their isothermal counterparts at this body location.

The results for the Le = 1.4 and the SCEBD model are quite similar and not reproduced here.

IV.   Conclusions

The film coefficient engineering model for evaluating aerothermal heating to a non-ablating, non-decomposing thermal protection system in a laminar, chemically reacting, dissociated flow is presented. Extensions to the film coefficient model such as mass injection, blowing, roughness augmentation, etc. were not assessed. The following conclusions may be drawn.

Edge properties

1. For a given body point, for a given trajectory point, the recovery enthalpy is essentially constant and insensitive to the tested assumptions. One exception is an extremely hot wall (i.e. $T_w >> T_e$) which can cause convective heating from the vehicle to the boundary layer at downstream locations.

2. The recovery factor is approximately constant for the tested set of assumptions and in the streamwise direction, due to the Prandtl number model.

Diffusion model

1. Generally, the SCEBD model produced higher film coefficients, followed by the Le = 1.4 and then the Le = 1.

2. Non-equilibrium wall enthalpy based film coefficients at the stagnation point (severe conditions) showed divergent behavior between the three diffusion models, attributable to the rate of increase of the mass diffusion term relative to the rate of decrease of the conduction term.

Mass boundary condition

1. Chemical equilibrium is not necessarily ensured with a kinetic model, even at harsh flight conditions.

2. The degree of non-equilibrium at the wall will increase the film coefficient heat flux prediction if the non-equilibrium wall enthalpy is greater than the equilibrium wall enthalpy, and conversely, decrease the heat flux prediction if the non-equilibrium wall enthalpy is less than the equilibrium wall enthalpy.

American Institute of Aeronautics and Astronautics

3. At high wall temperatures, the choice of heterogeneous models paired with an equilibrium wall enthalpy can produce unphysically large film coefficient values.

4. The conduction term and the mass diffusion term are inversely related to one another. As the wall temperature increases, the heterogeneous rates will increase (and in the case of recombination, release energy), while the thermal gradient decreases. This process should be limited by chemical equilibrium, which depends on the chosen model for a mass boundary condition.

Energy boundary condition

1. Cold wall temperatures in nearly all cases produce material response heat fluxes conservative compared to the CFD predicted heat flux. The caveat associated with this boundary condition is the steep gradients produced by the low wall temperature, which may affect other boundary layer properties (such as integrated values to determine transition).

2. Hot wall temperatures under certain sets of assumptions will produce non-physical results and should be avoided when using the film coefficient model.

3. Radiative equilibrium BC produces a thermal distribution as a function of streamwise direction which increases the available energy at downstream body locations on the vehicle (relative to an isothermal solution).

Design considerations

1. The recommended energy boundary condition in the CFD simulations used to generate film coefficients is the radiative equilibrium boundary condition. It generates a physics model dependent surface solution along the vehicle which provides non-arbitrary approximations of important boundary layer phenomena, such as thermal gradients and upstream energy transport. In most instances along the trajectory, this approximation will yield a wall temperature closer to the material response wall temperature, which ensures small corrections within the film coefficient model.

2. A non-equilibrium (CFD-calculated) wall enthalpy should be used to calculate the film coefficient. This provides a normalizing energy potential which most accurately matches the provided heat flux. In the instance of 5-species air, the higher energetic dissociated atoms decrease the potential which leads to higher valued film coefficients, and thus a built-in factor of safety for design.

3. The choice of catalytic behavior will depend upon the vehicle and the material for the specific body point. As seen in this body of work, a non-catalytic material can be modeled with a non-catalytic wall, with an expected margin of conservatism. This, however, does not include catalytic overshoot which

occurs at material interfaces of non-catalytic to catalytic materials. For highly reactive surfaces, a fully catalytic model limited by chemical equilibrium is preferred to avoid non-physical complications at higher wall temperatures.

Future Work

A primary focus of this investigation is to inform future aerothermal design of spacecraft. The majority of this analysis was conducted for a single flight condition and flight configuration. It may be extended to further flight space and numerous flight configurations, such as lifting or slender bodies, as appropriate for application. The flow field may also be varied in a myriad of different ways, including changes to the transport models, separated or turbulent flow, and coupling to radiation codes. Of particular interest may be the continued analysis of diffusion vs. conduction effects as a function of wall temperature when better surface reaction models are available to characterize surface catalysis. It is also worth mentioning that nonlinear temperature dependent catalysis models (such as proposed by Stewart[39]) can lead to a non-conservative film coefficient.

V.   Acknowledgements

References

[1]Martin, A. and Boyd, I. D., "Strongly coupled computation of material response and nonequilibrium flow for hypersonic ablation," *Journal of Spacecraft and Rockets*, Vol. 52, No. 1, January 2015, pp. 89–104.
doi:10.2514/1.A32847

[2]Culler, A. J. and McNamara, J. J., "Studies on fluid-thermal-structural coupling for aerothermoelasticity in hypersonic flow," *AIAA journal*, Vol. 48, No. 8, August 2010, pp. 1721–1738.
doi:10.2514/1.J050193

[3]Kuntz, D. W., Hassan, B., and Potter, D. L., "Predictions of ablating hypersonic vehicles using an iterative coupled fluid/thermal approach," *Journal of thermophysics and Heat Transfer*, Vol. 15, No. 2, 2001, pp. 129–139.
doi:10.2514/2.6594

[4]Zhang, H., *High Temperature Flow Solver For Aerothermodynamics Problems*, Ph.D. Thesis, University of Kentucky, Lexington, KY, July 2015.
doi:10.13023/etd.2015.002

[5]Zibitsker, A. L., McQuaid, J. A., Martin, A., and Brehm, C., "Fully-Coupled Simulation of Low Temperature Ablator and Hypersonic Flow Solver," *AIAA SciTech Forum*, AIAA Paper 2022-0676, Jan 2022.

doi:10.2514/6.2022-0676

[6]Kendall, R. M., Bartlett, E. P., Rindal, R. A., and Moyer, C. B., "An analysis of the coupled chemically reacting boundary layer and charring ablator. Part 1 - Summary Report," Contractor Report NASA-CR-1060, NASA, June 1968.
doi:2060/19680015772

[7]Moyer, C. B. and Rindal, R. A., "An analysis of the coupled chemically reacting boundary layer and charring ablator. Part 2 - Finite Difference Solution for the In-Depth Response of Charring Materials Considering Surface Chemical and Energy Balances," Contractor Report NASA-CR-1061, NASA, June 1968.
doi:2060/19680017220

[8]Bartlett, E. P. and Kendall, R. M., "An analysis of the coupled chemically reacting boundary layer and charring ablator. Part 3 - Nonsimilar solution of the multicomponent laminar boundary layer by an integral matrix method," Contractor Report NASA-CR-1062, NASA, June 1968.
doi:2060/19680017169

[9]Bartlett, E. P., Kendall, R. M., and Rindal, R. A., "An analysis of the coupled chemically reacting boundary layer and charring ablator. Part 4 - A unified approximation for mixture transport properties for multicomponent boundary-layer applications," Contractor Report NASA-CR-1063, NASA, June 1968.
doi:2060/19680017343

[10]Kendall, R. M., "An analysis of the coupled chemically reacting boundary layer and charring ablator. Part 5 - A General Approach to the Thermochemical Solution of Mixed Equlibrium-Nonequilibrium, Homogeneos or Heterogeneous Systems," Contractor Report NASA-CR-1064, NASA, June 1968.
doi:2060/19680017344

[11]Rindal, R. A., "An analysis of the coupled chemically reacting boundary layer and charring ablator. Part 6 - An Approach for characterizing Charring Ablator Response with In-Depth Coking Reactions," Contractor Report NASA-CR-1065, NASA, June 1968.
doi:2060/19680017345

[12]Eckert, E. and Drake, R. M., *Heat and Mass Transfer*, McGraw-Hill Book Company, 1959.

[13]Spalding, D., "A standard formulation of the steady convective mass transfer problem," *International Journal of Heat and Mass Transfer*, Vol. 1, No. 2-3, Aug 1960, pp. 192–207.
doi:10.1016/0017-9310(60)90022-3

[14]Kays, W. M., *Convective heat and mass transfer*, Tata McGraw-Hill Education, 2011.

[15]Cooper, J., "A Decoupled Engineering Methodology for Accurate Prediction of Ablative Surface Boundary Conditions in Thermal Protection Systems," 2022.

[16]Pohlhausen, K., "Zur näherungsweisen integration der differentialgleichung der iaminaren grenzschicht," *ZAMM-Journal of Applied Mathematics and Mechanics/Zeitschrift für Angewandte Mathematik und Mechanik*, Vol. 1, No. 4, 1921, pp. 252–290.

[17]Dorrance, W. H., *Viscous Hypersonic Flow: Theory of Reacting and Hypersonic Boundary Layers*, Dover Publications, July 2017.

[18]Eckert, E. and Drewitz, O., "The Heat Transfer to a Plate in Flow at High Speed," Technical Memorandum NACA-TM-1045 (Forschung Volume 11 Issue 3), NACA, Washington, 1943.
doi:2060/20050019476

[19]Eckert, E. R., "Survey on heat transfer at high speeds," Tech. Rep. AD0274109, Aeronautical Research Laboratory, Office Of Aerospace Research, United States Air Force, Minneapolis, MN, December 1961.
https://apps.dtic.mil/sti/citations/AD0274109

[20]Rubesin, M. W. and Johnson, H., "A critical review of skin-friction and heat-transfer solutions of the laminar boundary

layer of a flat plate," *Trans. ASME*, Vol. 71, No. 4, 1949, pp. 383–388.

[21]Von Driest, E. R., *The problem of aerodynamic heating*, Institute of the Aeronautical Sciences, 1956.

[22]Bianchi, D., Nasuti, F., Martelli, E., and Onofri, M., "A numerical approach for high-temperature flows over ablating surfaces," *39th AIAA Thermophysics Conference*, AIAA Paper 2007-4537, Miami, FL, June 2007.
doi:10.2514/6.2007-4537

[23]Martin, A., Zhang, H., and Tagavi, K. A., "An introduction to the derivation of surface balance equations without the excruciating pain," *International Journal of Heat and Mass Transfer*, Vol. 115, Part A, December 2017, pp. 992–999.
doi:10.1016/j.ijheatmasstransfer.2017.07.078

[24]Candler, G. V., "Nonequilibrium processes in hypervelocity flows: an analysis of carbon ablation models," *50th AIAA Aerospace Sciences Meeting*, AIAA Paper 2012-0724, Nashville, TN, January 2012.
doi:10.2514/6.2012-724

[25]Ramshaw, J. D., "Self-consistent effective binary diffusion in multicomponent gas mixtures," *Journal of Non-Equilibrium Thermodynamics*, Vol. 15, No. 3, 1990, pp. 295–300.
doi:10.1515/jnet.1990.15.3.295

[26]Goulard, R., "On catalytic recombination rates in hypersonic stagnation heat transfer," *Journal of Jet Propulsion*, Vol. 28, No. 11, November 1958, pp. 737–745.
doi:10.2514/8.7444

[27]Fay, J. A. and Riddell, F. R., "Theory of stagnation point heat transfer in dissociated air," *Journal of the Aerospace Sciences*, Vol. 25, No. 2, February 1958, pp. 73–85.
doi:10.2514/8.7517

[28]Lees, L., "Laminar heat transfer over blunt-nosed bodies at hypersonic flight speeds," *Journal of Jet Propulsion*, Vol. 26, No. 4, April 1956, pp. 259–269.
doi:10.2514/8.6977

[29]Park, C., "Numerical Implementation of Surface Catalysis, Reaction, and Sublimation," *Experiment, Modeling and Simulation of Gas-Surface Interactions for Reactive Flows in Hypersonic Flights*, Vol. RTO-EN-AVT-142, No. 16, 2007, pp. 16–1 – 16–20.

[30]Brandis, A. M. and Johnston, C. O., "Characterization of stagnation-point heat flux for earth entry," *45th AIAA Plasmadynamics and Lasers Conference*, AIAA Paper 2014-2374, Atlanta, GA, June 2014.
doi:10.2514/6.2014-2374

[31]Cooper, J. M., Stieha, J. K., Fowler, A. M., and Martin, A., "Kentucky Re-entry Universal Payload System," *54th AIAA Aerospace Sciences Meeting*, AIAA Paper 2016-2192, San Diego, CA, January 2016.
doi:10.2514/6.2016-2192

[32]Sutton, K. and Graves Jr., R. A., "A general stagnation-point convective heating equation for arbitrary gas mixtures," Technical Report NASA-TR-R-376, NASA, November 1971.
doi:2060/19720003329

[33]"US standard atmosphere 1976," Tech. Rep. NOAA-S/T-76-1562, National Oceanic and Atmospheric Administration, National Aeronautic and Space Administration, United States Air Force, Washington, D.C., October 1976.
doi:2060/19770009539

[34]Wright, M. J., Candler, G. V., and Bose, D., "Data-parallel line relaxation method for the Navier-Stokes equations," *AIAA journal*, Vol. 36, No. 9, September 1998, pp. 1603–1609.
doi:10.2514/2.586

[35]Gordon, S. and McBride, B. J., "Thermodynamic data to 20,000 K for monatomic gases," Technical Publication NASA/TP-1999-208523, NASA, June 1999.

doi:2060/19990063361

[36]Gupta, R. N., Lee, K.-P., Thompson, R. A., and Yos, J. M., "Calculations and curve fits of thermodynamic and transport properties for equilibrium air to 30000 K," Reference Publication NASA-RP-1260, NASA, September 1991.

doi:2060/19920002067

[37]Park, C., "Review of chemical-kinetic problems of future NASA missions. I-Earth entries," *Journal of Thermophysics and Heat transfer*, Vol. 7, No. 3, July 1993, pp. 385–398.

doi:10.2514/3.431

[38]Park, C., *Nonequilibrium hypersonic aerothermodynamics*, Wiley-Interscience, February 1990.

[39]Stewart, D. A., "Surface catalysis and characterization of proposed candidate TPS for access-to-space vehicles," Technical Memorandum NASA-TM-112206, NASA Ames Research Center, Moffett Field, CA, July 1997.

doi:2060/19970026958

American Institute of Aeronautics and Astronautics